Supporting Information

Successive Magnetic Transitions Enable an Utrawide Temperature Window of Zero Thermal Expansion in (Hf,Ti)Fe_{2+x}

Zhao Pan,[1,#,*] Haowei Zhou,[2,#] Chao Chen,[1,3,#] Yili Cao,[2,*] Xubin Ye,[1] Ruilong Wang,[3] Shogo Kawaguchi,[4] Xianran Xing,[2,*] and Youwen Long[1,*]

[1] Beijing National Laboratory for Condensed Matter Physics, Institute of Physics, Chinese Academy of Sciences, Beijing 100190, P.R. China

[2] Institute of Solid State Chemistry, Department of Physical Chemistry, University of Science and Technology Beijing, Beijing, 100083, P.R. China

[3] Key Laboratory for Intelligent Sensing System and Security of Ministry of Education, Department of Physics, Hubei University, Wuhan 430062, P.R. China

[4] Research and Utilization Division, Japan Synchrotron Radiation Research Institute (JASRI), SPring-8, 1-1-1 Kouto, Sayo-cho, Sayo-gun, Hyōgo 679-5198, Japan

[#]These authors contributed equally: Zhao Pan, Haowei Zhou, and Chao Chen

[*]Corresponding author. Email: zhaopan@iphy.ac.cn; yilicao@ustb.edu.cn; xing@ustb.edu.cn; ywlong@iphy.ac.cn.

Materials and Methods.

Sample preparation.

All $Hf_{0.6}Ti_{0.4}Fe_{2+x}$ (x = 0, 0.2, 0.54, 0.8, 3) samples were synthesized via arc melting under a high-purity argon atmosphere, using high purity ($\geqslant$99.9%) metal as raw material. To ensure compositional uniformity, each sample was remelted at least three times. Then the samples were wrapped in molybdenum foil, sealed in quartz tubes under an argon atmosphere, annealed at 1473 K for 3 days, and finally quenched in water. The alloy samples were ground into powder for synchrotron radiation X-ray diffraction (SXRD), neutron powder diffraction (NPD), magnetization measurements and Mössbauer spectrum test.

Characterization.

Temperature dependence of the SXRD experiments were conducted at the BL02B2 beamline of SPring-8 (Japan) using a wavelength of approximately 0.42 Å . Linear thermal expansion measurements of the alloy bulk were performed over the temperature range of 110 to 650 K using a thermal expansion meter (NETZSCH DIL402). The coefficient of linear thermal expansion is calculated using the equation: $\alpha_l = \frac{\triangle l}{l_0 \times \triangle T}$. Here, α_l is the coefficient of linear thermal expansion, $\triangle T$ is the temperature range, $\triangle l$ is the length change and l_0 is the initial length of the sample. Isothermal and thermomagnetic magnetic measurements were performed using a Physical Property Measurement System (PPMS, Quantum Design). The temperature dependence of magnetization was measured under a magnetic field of 500 Oe, while the maximum magnetic field for isothermal susceptibility measurements was 4 T. The Australian Nuclear Science and Technology Organization (ANSTO) performed temperature-dependent neutron powder diffraction (NPD) using a high-intensity neutron diffractometer (WOMBAT), operating at the wavelength of 2.41 Å. The Rietveld refinements for the SXRD and NPD data were carried out by using Fullprof software. to obtain crystal and magnetic structure. The Mössbauer absorption spectra of ^{57}Fe were obtained using standard transmission geometry with ^{57}Co source embedded in a rhodium matrix. Calibration was conducted

using an α-Fe foil, with isomeric shifts referenced to α-Fe. A GeminiSEM 300 (ZEISS, Germany) scanning electron microscope, equipped with an Ultim Max (Oxford, UK) EDS spectrometer, was employed for scanning electron microscopy (SEM) imaging and X-ray energy dispersive spectroscopy (EDS) elemental analysis. Atomic resolution scanning transmission electron microscopy (STEM) images and energy-dispersive X-ray spectroscopy (EDX) data were obtained using an advanced FEI Themis TEM instrument, which is equipped with a CEOS probe corrector and a Gatan image filter spectrometer.

Figures and Tables.

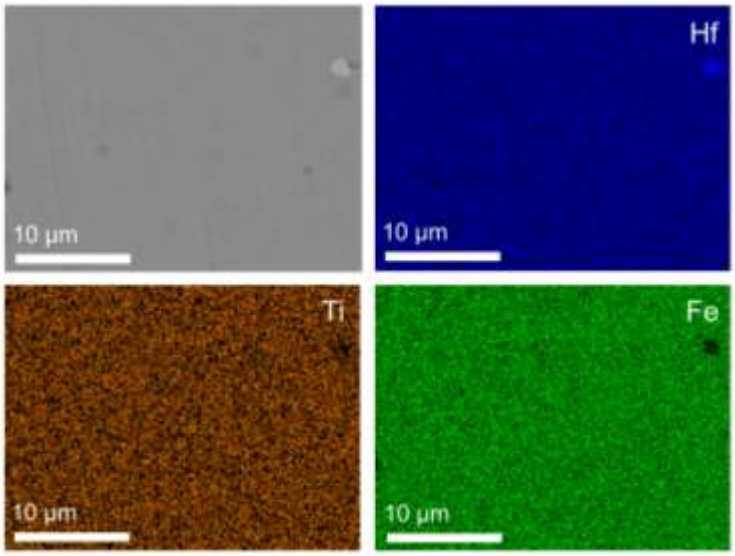

Figure S1. SEM images and EDS elemental maps of $Hf_{0.6}Ti_{0.4}Fe_{2.54}$ of Fe, Hf and Ti, which show uniform elemental distribution.

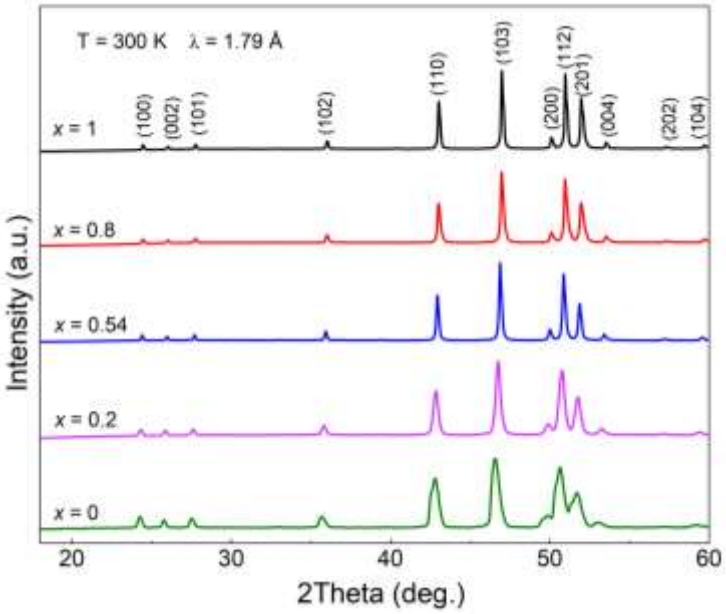

Figure S2. XRD patterns of $Hf_{0.6}Ti_{0.4}Fe_{2+x}$ (x = 0, 0.2, 0.54, 0.8, 1) samples.

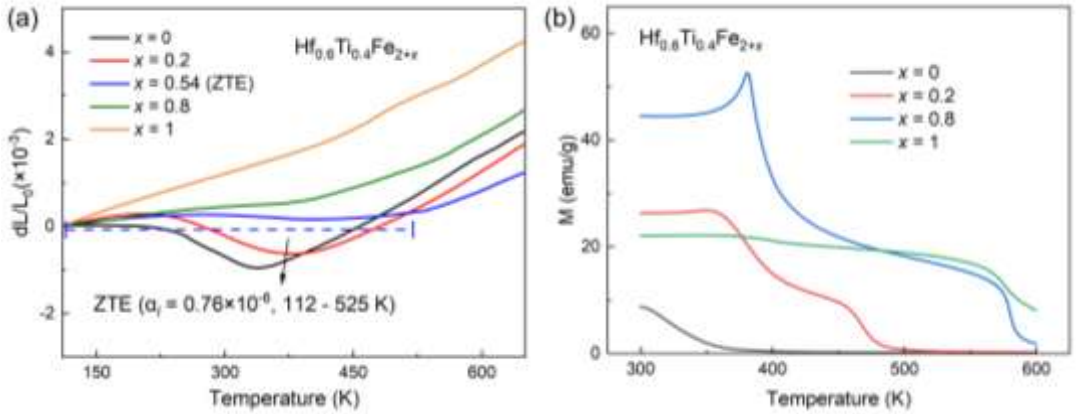

Figure S3. (a) Linear thermal expansion for $Hf_{0.6}Ti_{0.4}Fe_{2+x}$ (x = 0, 0.2, 0.54, 0.8, 1). (b) Temperature dependence magnetization with zero field cooled (ZFC) conditions for $Hf_{0.6}Ti_{0.4}Fe_{2+x}$ (x = 0, 0.2, 0.8, 1).

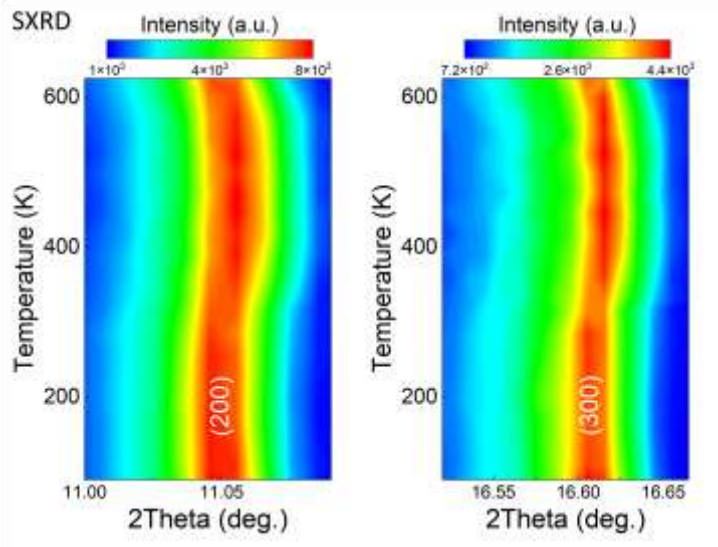

Figure S4. Temperature dependence of the SXRD peak (200) and (300) of $Hf_{0.6}Ti_{0.4}Fe_{2.54}$.

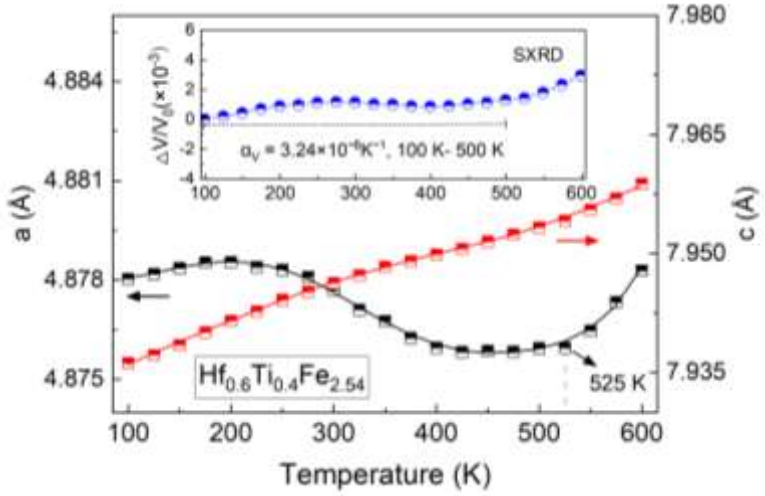

Figure S5. Temperature dependence of SXRD-measured lattice parameters and unit cell volume of $Hf_{0.6}Ti_{0.4}Fe_{2.54}$.

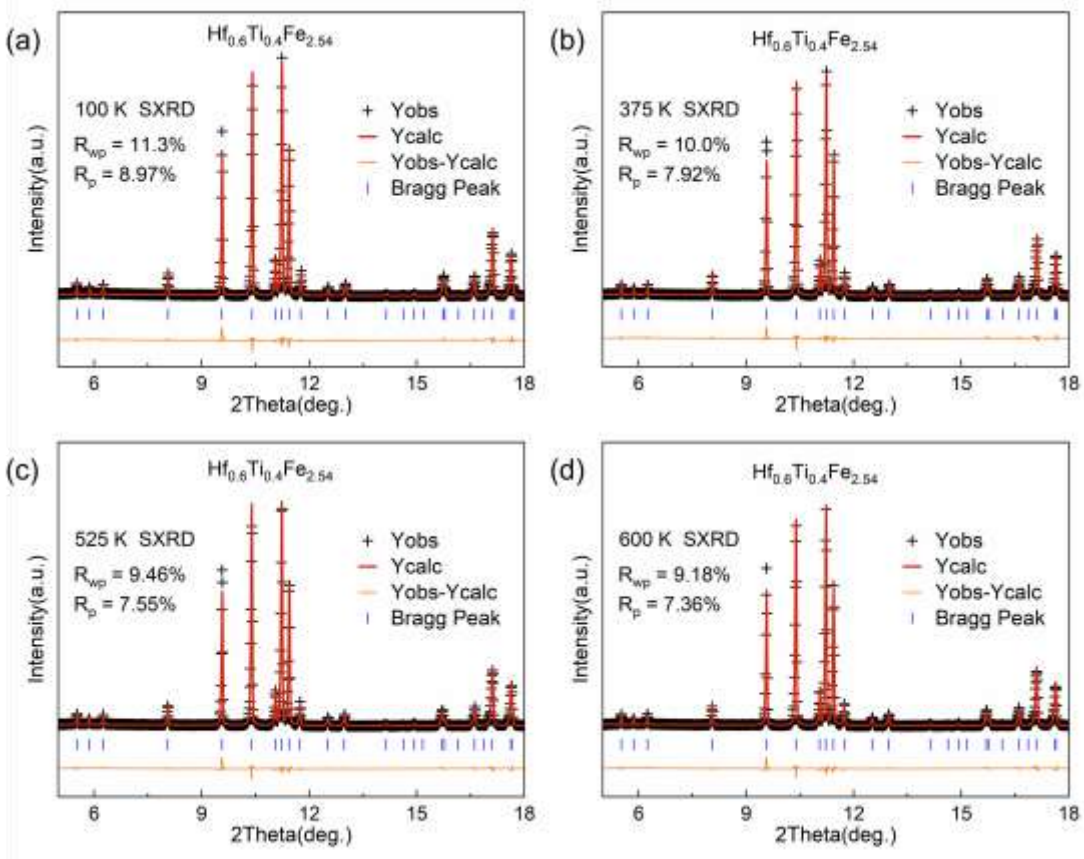

Figure S6. Synchrotron radiation X-ray diffraction refinement of $Hf_{0.6}Ti_{0.4}Fe_{2.54}$ at 100 K (a), 375 K (b), 525 K (c) and 600 K (d).

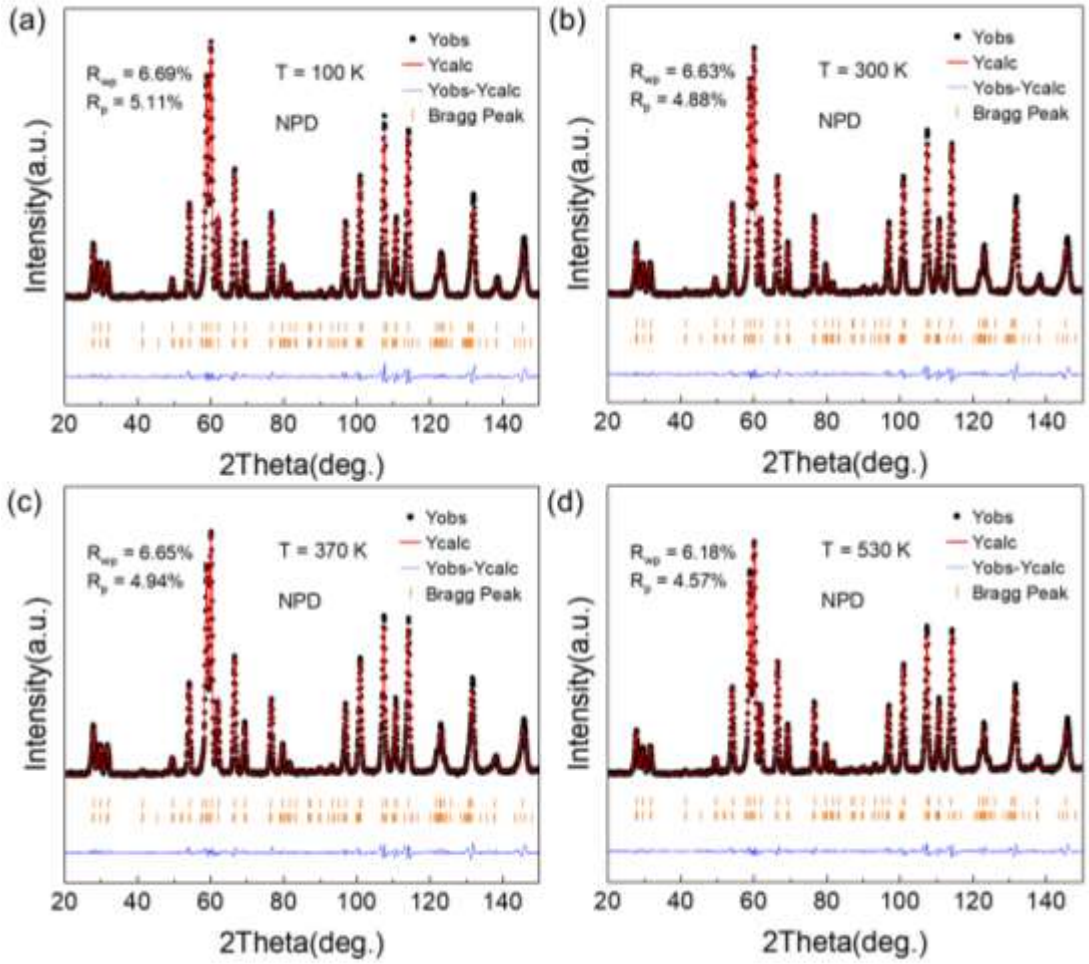

Figure S7. Neutron powder diffraction refinement of $Hf_{0.6}Ti_{0.4}Fe_{2.54}$ at (a) 100 K, (b) 300 K, (c) 370 K, and (d) 530 K.

Table S1. Temperature dependence of lattice parameters by SXRD patterns for $Hf_{0.6}Ti_{0.4}Fe_{2.54}$ compounds (100–600 K).

Temperature	a (Å)	c (Å)	V (Å^3)
100	4.87803 (7)	7.93621 (14)	163.543 (5)
125	4.87818 (7)	7.9372 (14)	163.573 (5)
150	4.87836 (7)	7.93845 (14)	163.611 (5)
175	4.87853 (7)	7.94007 (13)	163.656 (5)
200	4.87854 (7)	7.94153 (14)	163.687 (5)
225	4.87839 (7)	7.94271 (14)	163.701 (5)
250	4.87831 (7)	7.94416 (14)	163.725 (5)
275	4.87809 (7)	7.94518 (14)	163.732 (5)
300	4.8777 (7)	7.94629 (14)	163.728 (5)
325	4.8771 (7)	7.94725 (14)	163.708 (5)
350	4.87675 (7)	7.94831 (13)	163.706 (5)
375	4.87625 (7)	7.94902 (13)	163.687 (5)
400	4.87595 (7)	7.94986 (13)	163.684 (5)
425	4.87582 (7)	7.95058 (13)	163.690 (5)
450	4.87586 (7)	7.95153 (13)	163.713 (5)
475	4.87583 (7)	7.95238 (13)	163.728 (5)
500	4.87594 (7)	7.9533 (13)	163.75 (5)
525	4.87595 (7)	7.95411 (13)	163.772 (5)
550	4.87646 (7)	7.95552 (13)	163.835 (5)
575	4.87733 (7)	7.95694 (13)	163.923 (5)
600	4.87828 (7)	7.95879 (13)	164.025 (5)

Table S2. Temperature dependence of lattice parameters and atomic magnetic moment by NPD patterns for $Hf_{0.6}Ti_{0.4}Fe_{2.54}$ compounds (3−600 K).

Temperature	a (Å)	c (Å)	V (Å^3)	$M_{Fe\ (2a)}$ (μ_B)	$M_{Fe\ (6h)}$ (μ_B)	M_{total} (μ_B)
3	4.8823 (2)	7.93973 (4)	163.903 (1)	1.82 (10)	1.79 (6)	3.60 (14)
50	4.88211 (2)	7.94007 (5)	163.897 (1)	1.82 (11)	1.75 (6)	3.54 (15)
100	4.88233 (2)	7.94097 (5)	163.930 (1)	1.88 (8)	1.79 (5)	3.63 (12)
150	4.8826 (2)	7.94287 (5)	163.987 (1)	1.81 (10)	1.75 (6)	3.53 (14)
200	4.88278 (2)	7.94547 (5)	164.053 (1)	1.92 (8)	1.78 (5)	3.63 (12)
250	4.88283 (2)	7.94806 (5)	164.110 (1)	1.69 (11)	1.64 (7)	3.31 (16)
300	4.88239 (2)	7.95026 (5)	164.126 (1)	1.59 (11)	1.53 (7)	3.10 (16)
350	4.88158 (2)	7.95216 (5)	164.111 (1)	1.44 (12)	1.32 (8)	2.70 (18)
370	4.88118 (2)	7.95298 (5)	164.101 (1)	1.48 (12)	1.35 (7)	2.77 (18)
390	4.88072 (2)	7.95376 (5)	164.086 (1)	1.07 (9)	1.20 (11)	2.34 (21)
410	4.88048 (2)	7.95419 (5)	164.078 (1)	1.26 (9)	0.98 (13)	2.10 (24)
430	4.88028 (2)	7.95502 (5)	164.083 (1)	1.08 (9)	1.17 (11)	2.30 (22)
450	4.8802 (2)	7.95551 (5)	164.087 (1)	1.06 (9)	1.15 (10)	2.27 (20)
470	4.8802 (2)	7.95641 (5)	164.106 (1)	0.99 (9)	1.12 (10)	2.19 (20)
490	4.88036 (2)	7.95746 (5)	164.138 (1)	1.01 (9)	0.87 (13)	1.18 (25)
510	4.88058 (2)	7.95809 (5)	164.166 (1)	0.97 (11)	0.68 (17)	1.51 (32)
530	4.88073 (2)	7.9591 (5)	164.196 (1)	0.58 (13)	1.08 (12)	1.92 (25)
550	4.88107 (2)	7.96021 (5)	164.243 (1)	0	0	0
575	4.88199 (2)	7.96197 (5)	164.341 (1)	0	0	0
600	4.88315 (2)	7.96358 (5)	164.452 (1)	0	0	0

Table S3. Coefficient of thermal expansion, temperature windows and temperature windows $\triangle T$ (K) for some ZTE materials.

ZTE materials	Coefficient of thermal expansion	Temperature windows (K)	Temperature windows $\triangle T$ (K)	Reference
$Hf_{0.6}Ti_{0.4}Fe_{2.54}$	0.73×10^{-6} K^{-1} (α_l)	3-510	507	This work
$Tb_{0.6}Er_{0.4}Co_2Mn_{0.1}$	1.23×10^{-6} K^{-1} (α_l)	125-236	111	1
VB_2	2.18×10^{-6} K^{-1} (α_v)	5-150	145	2
$YbAl_{1.4}Mn_{0.6}$	1.64×10^{-6} K^{-1} (α_a)	140-300	160	3
$Tb(Co_{1.9}Fe_{0.1})$	0.48×10^{-6} K^{-1} (α_l)	123-307	184	4
$Gd_{0.5}(Ho_{0.5}Dy_{0.5})_{0.5}Co_2$	1.3×10^{-6} K^{-1} (α_l)	5-220	215	5
$Sc_{0.55}Ti_{0.45}Fe_2$	1.24×10^{-6} K^{-1} (α_v)	10-250	240	6
$Hf_{0.84}Ta_{0.16}Fe_{1.9}Cr_{0.1}$	1.55×10^{-6} K^{-1} (α_l)	110-370	260	7
$Gd_{0.25}Dy_{0.75}Co_{1.93}Fe_{0.07}$	0.16×10^{-6} K^{-1} (α_l)	10-275	265	8
$Dy(Co_{0.89}Fe_{0.11})_2$	0.58×10^{-6} K^{-1} (α_l)	5-305	300	9
(Ti, Zr, Hf, Nb, Fe)Fe_2	-0.62×10^{-6} K^{-1} (α_v)	10-360	350	10
$Zr_{0.8}Ta_{0.2}Fe_{1.7}Co_{0.3}$	0.21×10^{-6} K^{-1} (α_l)	5-360	355	11
$(Zr_{0.65}Nb_{0.35})_{0.95}Fe_{2.05}$	0.47×10^{-6} K^{-1} (α_a)	4-425	421	12
$Zr_{0.75}Nb_{0.25}Fe_2Co_{0.1}$	1.07×10^{-6} K^{-1} (α_a)	3-440	437	13
$Hf_{0.8}Nb_{0.2}Fe_{2.5}$	1.07×10^{-6} K^{-1} (α_l)	5-460	455	14
$Zr_{0.8}Nb_{0.2}Fe_2$	1.4×10^{-6} K^{-1} (α_l)	3-470	470	15
$Hf_{0.6}Ti_{0.4}Fe_{2.5}$	1.7×10^{-6} K^{-1} (α_v)	10-480	470	16

References.

1. Sun, Y.; Cao, Y.; Ren, Y.; Lapidus, S. H.; Li, Q.; Deng, J.; Miao, J.; Lin, K.; Xing, X. Structure, Magnetism and Low Thermal Expansion in $Tb_{1-x}Er_xCo_2Mn_y$ Intermetallic Compounds. *Microstructures* **2023**, *3*, 2023028.
2. Cao, Y.; Ji, W.; Lin, K.; Lin, H.; Li, Q.; Wang, C. W.; Wang, N.; Deng, J.; Chen, J.; Xing, X. Zero Thermal Expansion and Strong Covalent Binding of VB_2 Compound. *Inorg. Chem.* **2021**, *60* (14), 10095-10099.
3. Wang, H.; Xu, Y.; Song, Y.; Sanson, A.; Zhang, Y.; Yao, Y.; Liu, H.; Watanabe, T.; Zeng, J.; Shi, N.; Chen, J. Isotropic Zero Thermal Expansion in $Yb(Al,Mn)_2$: Achieving Continuous Shiftability over a Wide Temperature Range. *J. Am. Chem. Soc*. **2025**, *147* (38), 34697-34705.
4. Song, Y.; Chen, J.; Liu, X.; Wang, C.; Zhang, J.; Liu, H.; Zhu, H.; Hu, L.; Lin, K.; Zhang, S.; Xing, X. Zero Thermal Expansion in Magnetic and Metallic $Tb(Co,Fe)_2$ Intermetallic Compounds. *J. Am. Chem. Soc*. **2018**, *140* (2), 602-605.
5. Hao, J. Z.; Shen, F. R.; Hu, F. X.; Zhou, H. B.; Yu, Z. B.; Gao, Y. H.; Liang, W. H.; Qiao, K. M.; Wang, B. J.; Li, J.; Zhang, C.; Wang, J.; He, L. H, Liang, T. J.; He, J.; Sun, J. R.; Shen, B. G. Realization of Ultra-Low Thermal Expansion over a Broad Temperature Interval in $Gd_x(Dy_{0.5}Ho_{0.5})_{1-x}Co_2$ Compounds. *Scr. Mater.* **2020**, *185*, 181-186.
6. Song, Y.; Sun, Q.; Xu, M.; Zhang, J.; Hao, Y.; Qiao, Y.; Zhang, S.; Huang, Q.; Xing, X.; Chen, J. Negative Thermal Expansion in $(Sc,Ti)Fe_2$ Induced by an Unconventional Magnetovolume Effect. *Mater. Horiz*. **2020**, *7* (1), 275-281.
7. Zhou, C.; Wang, X.; Ai, M.; Long, F.; Zhong, H.; Lu, H.; Chen, J. Achieving Zero Thermal Expansion over a Wide Temperature Range in $(Hf,Ta)(Fe,Cr)_2$ Alloys. *Scierxiv*. **2025**, *5*, 2025097.
8. Hu, J.; Lin, K.; Cao, Y.; Yu, C.; Li, W.; Huang, R.; Fischer, H. E.; Kato, K.; Song, Y.; Chen, J.; Zhang, H.; Xing, X. Adjustable Magnetic Phase Transition Inducing Unusual Zero Thermal Expansion in Cubic RCo_2-Based Intermetallic Compounds (R = rare earth). *Inorg. Chem*. **2019**, *58* (9), 5401-5405.
9. Wang, J. N.; Hu, F. X.; Wang, B. J.; Tian, Z. Y.; Sun, C. Z.; Wang, J. T.; Huang, Q. Z.; Wang, J.; Chen, Y. Z.; Sun, J. R.; Zhao, T. Y.; Zhai, W.; Shen, B. G. Phase Transition Modulation and Wide Temperature Interval Zero Thermal Expansion in $Dy(Co_{1-x}Fe_x)_2$ Compounds. *Rare Met*. **2025**, *44*, 8911-8923.
10. Li, J.; Lin, K.; Xu, H.; Yang, W.; Zhang, Q.; Yu, C.; Zhang, Q.; Chen, J.; Wang, C. W.; Kato, K.; Kawaguchi, S.; You, L.; Cao, Y.; Li, Q.; Chen, X.; Miao, J.; Deng J.; Xing, X. High-Entropy Magnet Enabling Distinctive Thermal Expansions in Intermetallic Compounds. *J. Am. Chem. Soc*. **2024**, *146* (44), 30380-30387.
11. Li, W.; Lin, K.; Yan, Y.; Yu, C.; Cao, Y.; Chen, X.; Wang, C. W.; Kato, K.; Chen, Y.; An, K.; Zhang, Q.; Gu, L.; Deng, J.; Xing, X. A Seawater-Corrosion-Resistant and Isotropic Zero Thermal Expansion $(Zr,Ta)(Fe,Co)_2$ Alloy. *Adv. Mater*. **2022**, *34* (34), e2109592.
12. Sun, Y.; Cao, Y.; Hu, S.; Avdeev, M.; Wang, C. W.; Khmelevskyi, S.; Ren, Y.; Lapidus, S. H.; Chen, X.; Li, Q.; Deng, J.; Miao, J.; Lin, K.; Kuang, X.; Xing, X. Interplanar Ferromagnetism Enhanced Ultrawide Zero Thermal Expansion in Kagome Cubic Intermetallic $(Zr,Nb)Fe_2$. *J. Am. Chem. Soc.* **2023**, *145* (31), 17096-17102.

13. Sun, Y.; Yu, R.; Khmelevskyi, S.; Kato, K.; Cao, Y.; Hu, S.; Avdeev, M.; Wang, C.-W.; Yu, C.; Li, Q.; Lin, K.; Kuang, X.; Xing, X. Local Chemical Heterogeneity Enabled Superior Zero Thermal Expansion in Nonstoichiometric Pyrochlore Magnets. *Natl. Sci. Rev*. **2025**, *12* (3). nwae462.
14. Dong, X.; Yu, C.; Zhang, W.; Li, W.; Zhang, Q.; Liu, J.; Cao, Y.; Xing, X. Zero Thermal Expansion in Non-Stoichiometric and Single-Phase (Hf,Nb)$Fe_{2.5}$ alloy. *Scripta Mater.* **2023**, *229*, 115388.
15. Song, Y.; Sun, Q.; Yokoyama, T.; Zhu, H.; Li, Q.; Huang, R.; Ren, Y.; Huang, Q.; Xing, X.; Chen, J. Transforming Thermal Expansion from Positive to Negative: the Case of Cubic Magnetic Compounds of (Zr,Nb)Fe_2. *J. Phys. Chem. Lett*. **2020**, *11* (5), 1954-1961.
16. Lin, K.; Zhang, W.; Yu, C.; Sun, Q.; Cao, Y.; Li, W.; Jiang, S.; Li, Q.; Zhang, Q.; An, K.; Chen, Y.; Yu, D.; Liu, J.; Kato, K.; Zhang, Q.; Gu, L.; Kuang, X.; Tang, Y.; Miao, J.; Xing, X. Chemical Heterogeneity Modulated Zero Thermal Expansion Alloy over Super-Wide Temperature Range. *Cell Rep. Phys. Sci.* **2023**, *4* (2), 101254.